International Journal of Innovative Scientific & Engineering Technologies Research 14(3):169-187, July-Sept, 2026

© SEAHI PUBLICATIONS, 2026 www.seahipublications.org **ISSN: 2360-896X**

DOI:10.5281/zenodo.22663960

Substitutional Fe versus Mg Doping in Metastable Rock-Salt ZnO: First-Principles Formation Enthalpy and Thermodynamic Dopant Accessibility at the Zn Site

***[1]Hamman Mohammed Tampul, [2]Abubakar Umar Moreh & [2]Faruk Sani**

[1]Federal University Birnin Kebbi, Kebbi State, Nigeria
[2]Usmanu Danfodiyo University, Sokoto State, Nigeria
***Corresponding authors' email: tampulhamman@gmail.com**

ABSTRACT

Metastable rock-salt (B1) zinc oxide has attracted far less attention in doping thermodynamics than the wurtzite phase, and a direct first-principles comparison of transition-metal and alkaline-earth dopants on the Zn site under identical computational conditions is lacking. Using plane-wave density-functional theory with the revPBE functional, ultrasoft pseudopotentials, a 480 Ry kinetic-energy cutoff and a 20 × 20 × 20 k-point mesh within the Quantum ESPRESSO/thermo_pw workflow, we computed the formation energies of pristine, Fe-doped and Mg-doped B1 ZnO, modelling substitution as one neutral atom on a Zn site (25% concentration) of an eight-atom cell at the Zn-rich and O-rich limits of the ZnO chemical-potential window. With consistent per-atom normalisation of the elemental, oxygen and oxide reference states, the host formation enthalpy is −4.72 eV per formula unit on the physical oxide scale. Fe substitution is endothermic at the Zn-rich limit (+2.20 eV) and mildly exothermic at the O-rich limit (−2.52 eV); Mg substitution is exothermic at both limits (−2.83 and −7.55 eV), so Mg is the more accessible dopant by 5.03 eV under both conditions. The ordering is independent of the chemical-potential limit and survives the standard +1.36 eV per-O_2 correction, which shifts only the absolute O-rich values, and it reflects the stronger Mg–O bonding relative to ZnO. This study provides comparison between Fe and Mg substitution in B1 ZnO, establishing that Mg is a more thermodynamically accessible dopant than Fe at the Zn site.

Keywords: Rock-salt ZnO (B1 ZnO); defect formation energy; thermodynamic dopant accessibility; Fe versus Mg doping; Zn-rich and O-rich conditions.

1. INTRODUCTION

Zinc oxide (ZnO) remains one of the most intensively studied transparent semiconductors (Ahmedbowba et al., 2025): in its wurtzite phase it is a direct wide-gap material, whereas the rock-salt (B1) polymorph has a narrower, indirect band gap (Raha & Ahmaruzzaman, 2022; Segura et al., 2003). Its large exciton binding energy of 60 meV is favourable for room-temperature excitonic emission, and its combination of high transparency, piezoelectric response and chemical stability underpins applications ranging from transparent thin-film transistors and ultraviolet light-emitting diodes to gas sensors and transparent electrodes (Özgür et al., 2005). The material also lends itself to an extraordinary variety of nanoscale morphologies (Schmidt-Mende & MacManus-Driscoll, 2007).

At ambient conditions, ZnO crystallises in the wurtzite (B4) structure, but it transforms to the cubic rock-salt (B1) structure at roughly 10 GPa (Recio et al., 1998). The transition is a first-order phase transition and is accompanied by a volume collapse of about 18%, with the B1 lattice parameter and bulk modulus measured at a_0=4.280 Å and B_0=170 GPa (Gerward & Olsen, 1995). Calorimetric work shows the rock-salt polymorph to be metastable with respect to wurtzite by a standard enthalpy change $\Delta_{tr}H$=-11.7 $\pm$ 0.3 kJ/mol, which is $\Delta_{tr}H$=-0.121 $\pm$ 0.0031 eV per formula unit (Sharikov et al., 2017). The two structures are therefore energetically comparable within about 0.121 eV per formula unit even though their coordination environments differ fundamentally (tetrahedral (Figure 2) vs. octahedral (Figure 1)), and the B1 phase has an indirect band-gap electronic structure (Drissi et al., 2020).

Doping thermodynamics in ZnO is naturally formulated in terms of defect formation energies, which depend on the atomic chemical potentials set by the growth environment (Walle & Neugebauer, 2004; Zhang & Northrup, 1991). The formalism is standard and has been reviewed in considerable detail (Freysoldt et al., 2014); its application to ZnO has been reported for a large set of dopants in the wurtzite phase (Yim et al., 2017) and, for the rock-salt phase, in the context of p-type doping (Goyal & Stevanović, 2018). Iron is a particularly interesting dopant: Fe-doped ZnO has been studied experimentally and theoretically in connection with ferromagnetism, with Fe reported to occupy Zn sites in the 2+ and 3+ charge states depending on the compensating defect chemistry (Abdel-Baset et al., 2016); first-principles studies of Fe-doped ZnO clusters have likewise used chemical-potential-constrained formation energies to assess defect stability (Ganguli et al., 2009). Doping ZnO with Mg, by contrast, is a classical band-gap-engineering strategy: $Mg_xZn_{1-x}O$ alloys remain tetrahedrally coordinated (as illustrated in Figure 2) up to a Mg content of roughly 33%–40%, beyond which the rock-salt (sixfold-coordinated) structure becomes more stable (Maznichenko et al., 2009).

Most previous first-principles work on ZnO doping, however, has focused on the wurtzite phase. Systematic formation-energy data for metastable rock-salt B1 ZnO and, in particular, a direct comparison of a transition-metal and an alkaline-earth dopant under identical computational conditions remain comparatively scarce (Yim et al., 2017). Substitution energies in rock-salt differ from those in wurtzite because the surrounding oxygen atoms form an octahedral coordination environment (as shown in Figure 1). The purpose of the present work is to determine, from first principles, the total energies and formation energies of pristine, Fe-doped, and Mg-doped rock-salt (B1) ZnO at the Zn-rich and O-rich limits of the ZnO chemical-potential window, and to establish which dopant is thermodynamically more accessible in the B1 host.

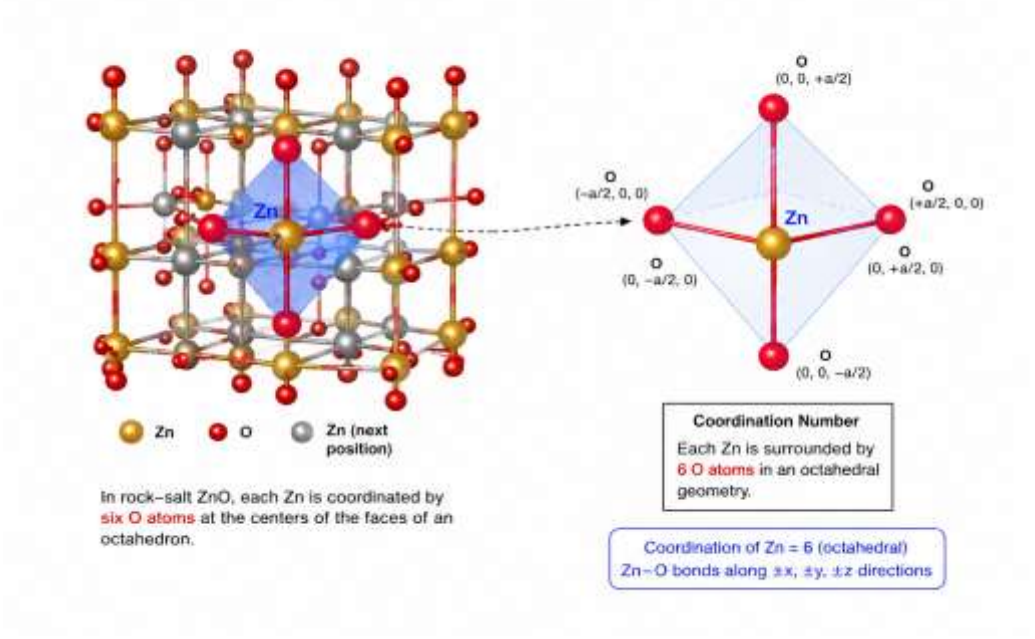

Figure 1. Octahedral coordination of oxygen around Zn in rock-salt ZnO

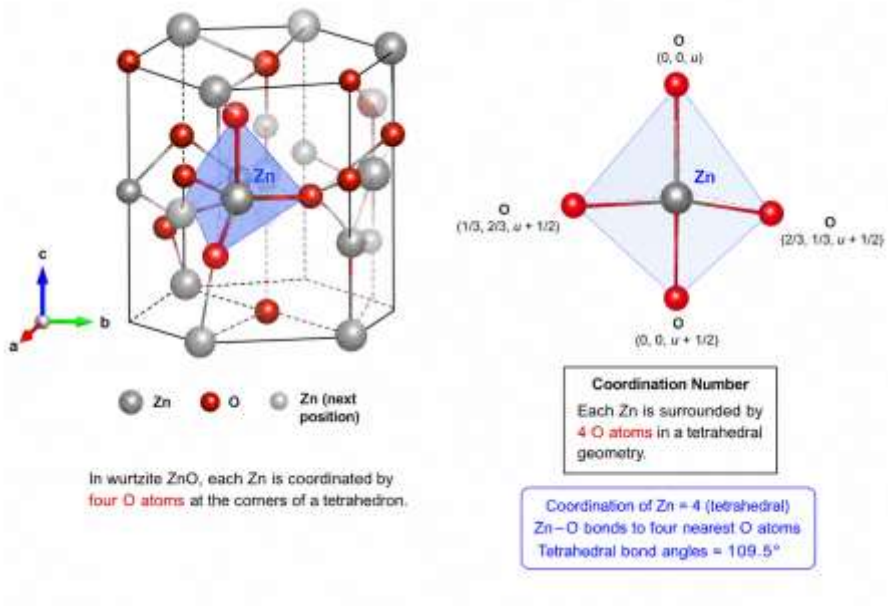

Figure 2. Tetrahedral coordination of oxygen around Zn in wurtzite ZnO

2. METHODOLOGY

2.1 Structural model

All calculations considered a cubic B1 rock-salt ZnO structure (space group $Fm\bar{3}m$) at 0 K and ambient pressure. The computational cell contains 4 Zn and 4 O atoms, i.e., 4 ZnO formula units. Substitutional doping was represented by replacing a single Zn atom with either Fe or Mg, which corresponds to 25%

Zn-site substitution as illustrated in Figure 3. The defects are electrically neutral, and no vacancies, interstitials, charged states, defect complexes or other defects are considered. It must be emphasised that the eight-atom cell is a bulk-like periodic supercell of B1 ZnO: it contains no surface and no finite-size particle morphology. No quantum confinement, surface or finite-size effects are present in the calculation, and the results describe the periodic bulk B1 phase.

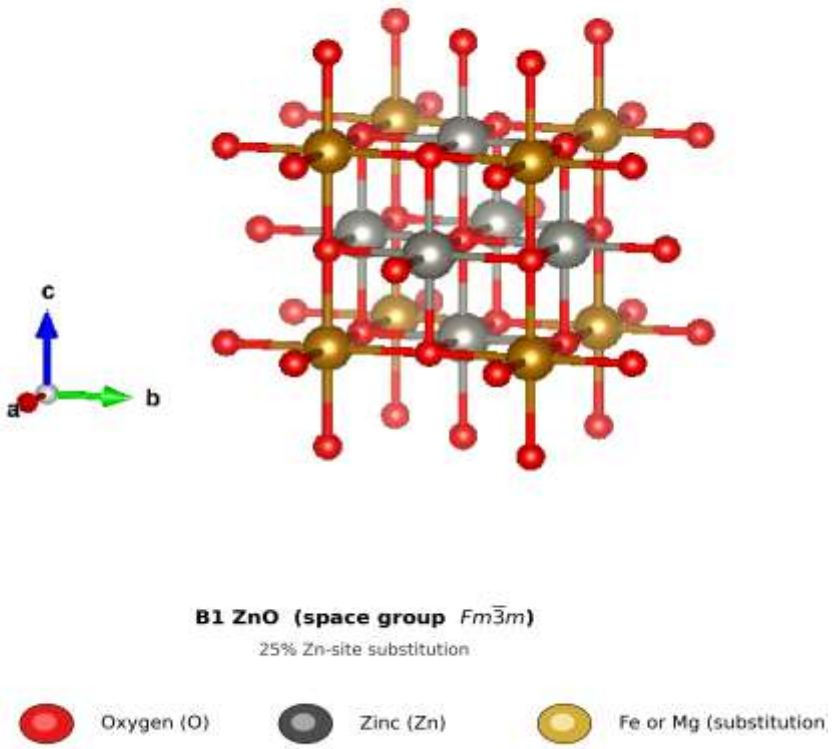

Figure 3. Ball-and-stick rendering of the B1 ZnO cell (space group Fm3̄m) with a 25% Zn-site substitution.

2.2 Computational parameters

The computational parameters are collected in Table 1, where the calculations are based on density-functional theory as formulated by Hohenberg & Kohn (1964) and Kohn & Sham (1965). The exchange–correlation energy is described by the revised Perdew–Burke–Ernzerhof (revPBE) generalised gradient approximation (the Zhang–Yang revision of PBE), which was introduced by Zhang and Yang to improve atomisation energetics (Hammer et al., 1999), built upon the parent PBE functional (Perdew et al., 1996). The Kohn–Sham orbitals are expanded in plane waves, and the electron–ion interaction is treated with ultrasoft pseudopotentials (Giannozzi et al., 2009) taken from the scalar-relativistic periodic table library of Corso (2014), generated with the atomic code (v. 6.4.1) for the revPBE functional using Troullier–Martins pseudization and including nonlinear core corrections. The oxygen pseudopotential treats a $2s^2 2p^4$ valence configuration with channel cutoff radii of 1.00 (s) and 0.90 (p) bohr, and carries suggested

minimum cutoffs of 47 Ry (wavefunctions) and 323 Ry (charge density). The zinc pseudopotential treats a $3s^2 3p^6 3d^{10} 4s^2$ valence configuration with cutoff radii of 0.80 (s), 1.00 (p) and 1.00 (d) bohr, and has suggested minimum cutoffs of 73 Ry (wavefunctions) and 394 Ry (charge density). The kinetic-energy cutoff is 480 Ry, which exceeds the higher of the two suggested wavefunction cutoffs (73 Ry), and the charge-density grid is likewise set above the higher suggested charge-density floor (394 Ry); the plane-wave representation is therefore converged with respect to the pseudopotential requirements of both species. The self-consistency threshold (conv_thr) is 1.0×10^{-8}, charge-density mixing uses mixing_beta 0.3, and the Brillouin zone is sampled with an automatic 20 × 20 × 20 Monkhorst–Pack-like mesh (K_POINTS AUTOMATIC 20 20 20 0 0 0, in Quantum ESPRESSO notation). Because ultrasoft pseudopotentials encode the functional used in their generation, all self-consistent field (SCF) runs use the same exchange–correlation functional as the pseudopotential flavour (Bartók & Yates, 2019); revPBE is therefore the functional label used consistently throughout this work.

Table 1. Computational parameters.

Parameter	Value
Exchange-correlation	GGA-revPBE (Zhang–Yang revision of PBE) (Hammer et al., 1999)
Electron-ion interaction	Plane-wave ultrasoft pseudopotentials (Giannozzi et al., 2009)
Code	Quantum ESPRESSO (thermo_pw workflow) (Giannozzi et al., 2017)
Kinetic energy cutoff	480 Ry
Self-consistency threshold (conv_thr)	1.0×10^{-8}
Charge density mixing (mixing_beta)	0.3
k-point mesh	20 × 20 × 20 (K_POINTS AUTOMATIC 20 20 20 0 0 0)
Structure	B1 rock-salt ZnO, space group Fm-3m
Cell	4 Zn + 4 O atoms (4 formula units)
Defects	Neutral substitutional Fe_Zn, Mg_Zn; 1 of 4 Zn sites (25%)
Conditions	0 K, ambient pressure

2.3 SCF Calculations

Self-consistent field (SCF) total energies were obtained for the pristine, Fe-doped, and Mg-doped B1 ZnO cells and for the elemental reference cells and the oxygen reference cell. In addition to the total energies, the SCF runs for the three oxide cells report the highest-occupied-level eigenvalues of 13.5861 eV (Fe-doped), 10.8342 eV (pristine), and 10.2717 eV (Mg-doped). These eigenvalues are referenced to the pseudopotential-defined energy zero and carry no thermodynamic meaning in this work; they are reported only for completeness.

2.4 Defect formation energy

Throughout this work, $E_{tot}[\cdot]$ denotes an SCF total energy, μ_i^{ref} the per-atom reference chemical potential of elemental species i (Zn, Fe, Mg metals; oxygen reference cell), μ_{ZnO} the total energy of B1 ZnO per formula unit, and μ_i^{limit} the chemical potential of species i at a given thermodynamic limit.

For a neutral substitutional defect X on a Zn site (X = Fe, Mg), the formation energy is defined, following the standard thermodynamic formalism (Freysoldt et al., 2014), as in Equation (1).

$$E_f(X_{Zn}) = E_{tot}[X\text{-doped ZnO}] - E_{tot}[ZnO] - \mu_X^{ref} + \mu_{Zn} \quad (1)$$

where $E_{tot}[X\text{-doped ZnO}]$ and $E_{tot}[ZnO]$ are the DFT total energies of the doped and pristine cells, respectively; μ_X^{ref} is the chemical potential of the dopant reservoir; and μ_{Zn} is the chemical potential of the removed Zn atom, which is set by the thermodynamic environment. A negative E_f indicates that substitution is exothermic with respect to the chosen reservoirs; a positive E_f indicates an endothermic process whose equilibrium concentration is exponentially suppressed at low temperature.

A distinction that deserves emphasis is that between the defect formation energy, given by Equation (1), and the compound formation energy of the ZnO host itself in Equation (2).

$$\Delta H_f(ZnO)=\mu_{ZnO}-\mu_{Zn}^{ref}-\mu_0^{ref}, \quad (2)$$

Equation (2) quantifies the stability of ZnO relative to its elemental references. The two quantities, the defect formation energy $E_f(X_{Zn})$ of Equation (1) and the compound formation energy $\Delta H_f(ZnO)$ of Equation (2), must not be confused; the large negative SCF total energies listed in Table 2 are neither of them. Absolute DFT total energies depend on the reference state, the pseudopotential, the atom count and the functional; only appropriately balanced energy differences, such as those of Equations (1) and (2), possess thermodynamic meaning.

2.5 Chemical-potential limits

At equilibrium between ZnO and its elements, the cation and anion chemical potentials obey the stability relation in Equation (3) (Sakong et al., 2013):

$$\mu_{Zn}+\mu_0=\mu_{ZnO}, \quad (3)$$

Here, $\mu_{ZnO}=E_{tot}[\text{ZnOcell}]/4$ is defined per formula unit. The condition that ZnO does not decompose into Zn metal or O_2 gas restricts μ_{Zn} and μ_0 to an allowed stability window whose two ends are the limiting conditions (Momot et al., 2017):

- **Zn-rich:** the Zn reservoir is crystalline Zn metal, $\mu_{Zn}=\mu_{Zn}^{ref}=E_{tot}[\text{Zncell}]/4=-6177.72639$ eV/atom; μ_0 is then fixed by $\mu_0^{\text{Zn-rich}}=\mu_{ZnO}-\mu_{Zn}^{ref}=-441.63$ eV/atom. Physically, this corresponds to growth in the presence of excess metallic Zn, in which case the oxygen chemical potential is depressed to the value at which ZnO is just stable against decomposition into Zn metal and O_2.
- **O-rich (O_2-gas-saturated):** the oxygen reservoir is molecular O_2, $\mu_0=\mu_0^{ref}=E_{tot}[\text{Ocell}]/8=-436.90506$ eV/atom (this identification with $\frac{1}{2}E(O_2)$ *should be verified against a gas-phase O_2 calculation in the same setup, as it is the premise on which the O-rich*

limit rests);μ_{Zn} follows from: $\mu_{Zn}^{\text{O-rich}}=\mu_{ZnO}-\mu_{O}^{ref}$ =-6182.44723 eV/atom. This is the limit relevant to oxidative growth conditions, and it is the only limit that enters the oxygen-reference analysis discussed in Section 2.6.

The two limits bracket the entire thermodynamically allowed range $\mu_O \in [\frac{1}{2}\mu_{O_2}+\Delta H_f(ZnO), \frac{1}{2}\mu_{O_2}]$, *i.e.,* *numerically* $\mu_O \in$ [-441.63,-436.91] eV/atom; equivalent conventions were used in the ZnO defect literature (Petretto & Bruneval, 2014; Yim et al., 2017).

2.6 Oxygen-reference treatment

Semi-local functionals like PBE and its revPBE revision used here are known to describe the O_2 molecule inaccurately, overbinding it and thereby biasing oxygen chemical potentials and oxide formation energies (Wang et al., 2006). The magnitude of the overbinding is implementation- and setup-dependent (0.96 eV per molecule in one GGA implementation (Mellan & Grau-Crespo, 2012)), and the standard remedy is a fitted upward shift of the O_2 energy: +1.36 eV per O_2 molecule in the widely used Wang–Maxisch–Ceder procedure (Wang et al., 2006); about +1.05 eV for the tetravalent oxides HfO_2, ZrO_2, TiO_2, SiO_2 and GeO_2 (Mellan & Grau-Crespo, 2012); and a +1 eV shift that brings the PBE formation enthalpy of wurtzite ZnO to −3.41 eV, close to experiment (Muller et al., 2022).

For the present work, a more fundamental statement takes precedence: the oxygen reference is an SCF output of our specific setup, and the consistency of the reference chain must be demonstrated before any interpretation. To obtain the reference oxygen chemical potential μ_O^{ref}, the total energy of the oxygen simulation cell is divided by the number of oxygen atoms it contains. The cell holds eight O atoms, so $\mu_O^{ref}=E_{tot}/8$=-3495.24046444/8=-436.90505805 eV/atom.

These three reference values, μ_O^{ref}, μ_{Zn}^{ref}, and μ_{ZnO}, must satisfy Equation (2), written for the formation reaction $Zn+\frac{1}{2}O_2 \rightarrow ZnO$ *as* $\Delta H_f=\mu_{ZnO}-\mu_{Zn}^{ref}-\mu_O^{ref}$. With μ_O^{ref}=-436.90506 eV/atom, μ_{Zn}^{ref}=-24710.90555585/4=-6177.72639 eV/atom (four Zn atoms in the Zn crystal cell) and μ_{ZnO}=-6619.35229 eV per formula unit (B1 ZnO, four formula units per cell), Equation (2) gives rise to Equation (4).

$$\Delta H_f=-6619.35229-(-6177.72639)-(-436.90506)=-4.72\text{eV per formula unit.} \quad (4)$$

This single value ties the metal, the oxygen reference and the crystal zinc oxide together, confirming that all reference calculations followed a comparable protocol before any substitution energetics is considered. The computed compound formation enthalpy can be checked against experiment by a two-step argument. First, direct calorimetry of the phase transition from the rock-salt to the wurtzite structure in ZnO gives $\Delta_{tr}H=-11.7\pm0.3$ kJ/mol, which means B1 ZnO is less stable than wurtzite by about 0.12 eV per formula unit (Sharikov et al., 2017). Second, the experimental formation enthalpy of wurtzite ZnO is well established at approximately −347 to −351 kJ/mol, i.e., roughly −3.6 eV per formula unit (Itoh & Azakami, 1989). Combining the two statements, a physically consistent formation enthalpy for B1 ZnO must fall near the wurtzite value, shifted by the small metastability penalty of about 0.12 eV per formula unit that is, within the −3 to −4 eV per formula unit window. The SCF reference chain yields −4.72 eV per formula unit as seen in Equation (4), on the expected oxide scale, but somewhat more negative than the −3 to −4 eV window typical of semi-local descriptions. The offset, of order 1 eV per formula unit, is

attributable to the precise definition and normalisation of the oxygen reference used here and is quantified in Sections 3.2 and 3.8.

For the same reason, no literature value can substitute for the SCF reference without importing a second energy reference. Fitted correction schemes, such as the +1.36 eV shift for O_2 (Friedrich et al., 2019; Wang et al., 2006), the fitted-elemental-reference-energies approach (Stevanović et al., 2012), or the Open Quantum Materials Database oxygen reference of −4.52 eV with its stated 0.2 eV uncertainty (Baldassarri et al., 2023), are tuned to specific functionals, pseudopotentials and fitting sets; the fitted value depends so strongly on the simulation parameters that one must either reuse the original fitting parameters or repeat the fitting (Youssef & Yildiz, 2012). This caution is sharpened here by the revPBE functional of the present pseudopotentials, which diverges from the plain-PBE fits on which most published corrections rest. One property of any such correction remains useful: it shifts all oxygen-referenced quantities by a constant and leaves differences between similarly referenced quantities unchanged (Baldassarri et al., 2023). Accordingly, this work reports the raw SCF results in full, and Section 3.8 evaluates the effect of the standard +1.36 eV correction to document its suitability for the present data.

2.7 Computational workflow

Total energies were obtained within the Quantum ESPRESSO suite under the thermo_pw workflow, an open collection of drivers that call Quantum ESPRESSO PWscf and Phonon routines to compute total energies and, where required, derived thermodynamic quantities (Giannozzi et al., 2017). The workflow used here comprises: (i) SCF calculations of the three oxide cells and the four reference cells; (ii) conversion of total energies between Rydberg and electronvolt; (iii) normalisation of the multi-atom reference cells to per-atom (and per-formula-unit) chemical potentials; (iv) evaluation of the ZnO stability relation, Equation (3), and of both chemical-potential limits; and (v) evaluation of Equation (1) for all combinations. Every numerical step was verified independently in both Ry and eV units, as detailed in Section 3.1 and tabulated in Table 2.

3. RESULTS AND DISCUSSION

3.1 Total energies, reference-state normalisation and dataset consistency

The SCF total energies of the ZnO cells are E_{tot} =-1946.05269514 Ry (pristine), -1739.61375727 Ry (Fe-doped ZnO) and -1618.68846370 Ry (Mg-doped ZnO), together with the highest-occupied-level eigenvalues quoted in Section 2.3.

The conversion factor between units is 1 Ry = 13.605693 eV. Multiplying the Rydberg energy values reproduces the supplied electronvolt values to within rounding of the conversion constant, confirming internal consistency of the conversion.

Table 2 collects all total energies and the normalised reference chemical potentials. Each elemental cell contains four atoms, so the elemental chemical potentials are the cell energies divided by four; the oxygen reference cell contains eight O atoms, so the oxygen chemical potential is $E_{tot}/8$. Using a raw multi-atom cell total energy directly as a chemical potential would be a normalisation error of precisely this kind, and all quantities below use the per-atom (per-molecule, per-formula-unit) values.

Table 2. SCF total energies and normalised reference chemical potentials.

System (cell)	E_{tot} /(Ry)	E_{tot} /(eV)	Normalisation	μ /(eV)
ZnO, pure (4 Zn, 4 O)	-1946.05	-26477.41	per formula unit	−6619.35229 eV/f.u.
ZnO, Fe-doped	-1739.61	-23668.66	—	—
ZnO, Mg-doped	-1618.69	-22023.39	—	—
Zn crystal (4 atoms)	-1816.22	-24710.91	per atom	−6177.72639 eV/atom
Fe crystal (4 atoms)	-991.11	-13484.71	per atom	−3371.17660 eV/atom
Mg crystal (4 atoms)	-505.93	-6883.49	per atom	−1720.87351 eV/atom
O reference (8 atoms)	-256.9	-3495.24	per atom	−436.90506 eV/atom

3.2 ZnO chemical-potential stability window

With μ_{ZnO}=-26477.40915427/4=-6619.35229 eV per formula unit, μ_{Zn}^{ref}=-24710.90555585/4=-6177.72639 eV/atom and μ_{O}^{ref}=-3495.24046444/8=-436.90506 eV/atom, Equation (4) gives a compound formation enthalpy of −4.72 eV per formula unit, and hence a stability window $\mu_O \in$ [-441.63,-436.91] eV, as shown in Figure 4; equivalently, in the reduced form by Meyer (2004), the relative stability condition is $\Delta\mu_O \in$ [-4.72,0] eV. The physical content of this value is transparent: after normalisation, the oxygen in ZnO is stabilised by approximately 4.72 eV per atom (as depicted in Figure 4) relative to the per-atom oxygen reference: a statement about the compound, not about any defect, and precisely the quantity that sets the width of the window in Figure 4.

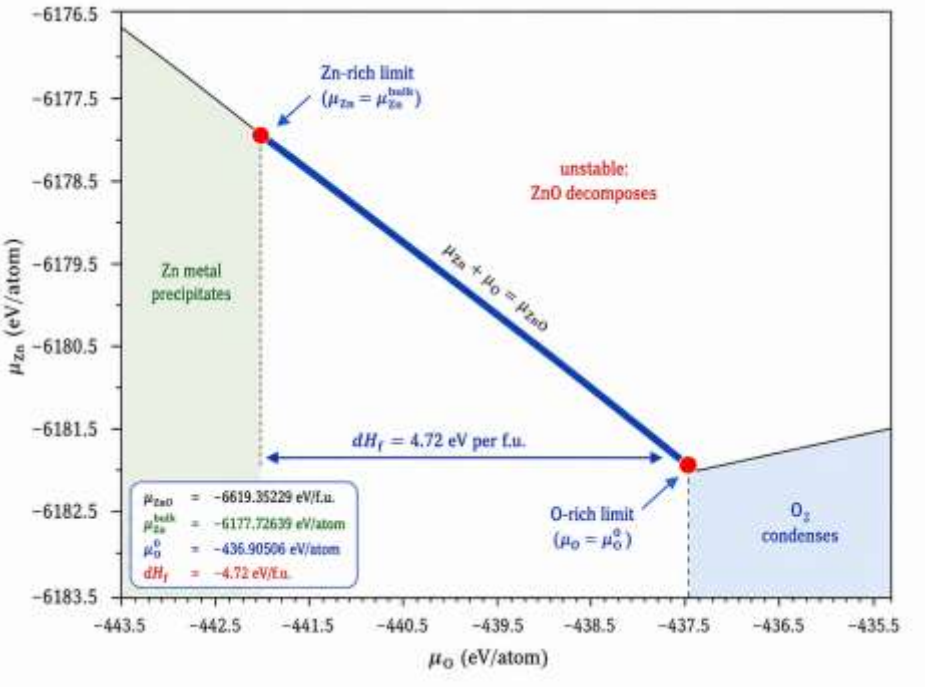

Figure 4. Thermodynamic stability window of B1 ZnO in the (μ_{Zn}, μ_O) chemical-potential plane. The width of the window (4.72 eV) equals the compound formation enthalpy.

This result withstands scrutiny. Well-established experimental thermochemistry gives $\Delta_f H^\circ(ZnO, s, 298\text{K}) \approx$ -347kJ/mol to −351 kJ/mol, i.e., about −3.6 eV per formula unit (Itoh & Azakami, 1989); diffusion quantum Monte Carlo calculations place the wurtzite formation enthalpy near −3.94 eV or −4.15 eV (Santana et al., 2015); and PBE calculations of ZnO formation enthalpies reported in the literature cluster around −2.96 eV (Petretto & Bruneval, 2014) and −3.12 eV (Momot et al., 2017), with the corrected PBE value for wurtzite ZnO at −3.41 eV (Müller et al., 2022). Since the B1 phase lies only about 0.1 eV per formula unit above wurtzite (Sharikov et al., 2017), a value of −4.72 eV per formula unit sits on the physically expected oxide scale, though it is more negative by roughly 1 eV than the −3 to −4 eV window typical of semi-local descriptions; the origin of this offset is analysed in Section 3.8.

3.3 Formation energy of pristine B1 ZnO

The formation energy of the pristine host per formula unit is precisely the compound formation enthalpy of Equation (4), −4.72 eV per formula unit (equivalently −18.88 eV for the four-formula-unit cell). It does not depend on which chemical-potential limit is chosen, since the limits only re-partition μ_{Zn} and μ_O under the constraint of Equation (3); the pristine cell is the thermodynamic reference against which all doping energies are measured. Two consequences follow. First, the magnitude of ΔH_f, which is not a defect property, controls the difference between the Zn-rich and O-rich defect formation energies. Second, because the O-rich μ_{Zn} is obtained from Equation (3) using the same μ_{ZnO}, the compound formation enthalpy enters every O-rich result directly. The Zn-rich defect energies, in contrast, do not involve μ_{ZnO} in the removed-atom term, since μ_{Zn}=μ_{Zn}^{ref} is fixed directly by the metal.

3.4 Fe substitution at the Zn site

Using Equation (1) with μ_{Fe}^{ref}=-13484.70638994/4=-3371.17660 eV/atom:

- **Zn-rich:** $E_f(Fe_{Zn})$=-23668.66289729-(-26477.40915427)+3371.17660-6177.72639=+2.20 eV.
- **O-rich:** $E_f(Fe_{Zn})$=+2.20+($\mu_{Zn}^{O\text{-rich}}$-μ_{Zn}^{ref})=+2.20-4.72=-2.52 eV.

At the Zn-rich limit, Fe substitution is endothermic by +2.20 eV: Fe_2O_3-type oxide chemistry notwithstanding, substituting a Zn atom with Fe referenced to the Fe metal crystal is energetically costly under Zn-saturated conditions, and the equilibrium Fe fraction in B1 ZnO would be small at 0 K. At the O-rich limit, Fe substitution becomes mildly exothermic (−2.52 eV): the shift of μ_{Zn} by the compound formation enthalpy (−4.72 eV) is exactly the thermodynamic cost of removing Zn from a host grown in an oxygen-saturated environment, and the equilibrium Fe fraction would accordingly be larger at the O-rich limit than at the Zn-rich limit.

3.5 Mg substitution at the Zn site

With μ_{Mg}^{ref}=-6883.49404682/4=-1720.87351 eV/atom:

- **Zn-rich:** $E_f(Mg_{Zn})$=-22023.38963056-(-26477.40915427)+1720.87351-6177.72639=-2.83 eV.
- **O-rich:** $E_f(Mg_{Zn})$=-2.83+($\mu_{Zn}^{O\text{-rich}}$-μ_{Zn}^{ref})=-2.83-4.72=-7.55 eV.

Mg substitution is therefore exothermic at both the Zn-rich and the O-rich limits. This is not surprising in chemical terms: Mg–O bonds are among the strongest of the simple oxides (Doerksen & Fortenberry, 2020), and revPBE correctly captures that MgO is more stable than ZnO relative to their elemental references, the same driving force that places the wurtzite-to-rock-salt boundary in $Mg_xZn_{1-x}O$ near $x \approx 0.33$ (Maznichenko et al., 2009). No spin-polarisation issue arises for the closed-shell Mg^{2+} configuration (Utrera-Barrios et al., 2023), so the Mg numbers require no magnetic qualification of the kind that applies to Fe.

3.6 Fe versus Mg thermodynamic accessibility

Within the defect-thermodynamics framework of this research, a dopant is more accessible when, under identical chemical-potential conditions and reference states, its substitution formation energy is lower, corresponding to higher equilibrium solubility at a given temperature within the validity of the 0 K, dilute-to-25% modelling. By that definition, Mg is decisively the more accessible dopant in B1 ZnO at both limits. Equation (5) shows that Mg substitution is 5.03 eV more favourable than Fe substitution at the Zn-rich limit and remains significantly more stable at the O-rich boundary (Section 3.5).

$$E_f(Mg_{Zn})-E_f(Fe_{Zn})=-5.03eV, \quad (5)$$

The constancy of this difference (in Table 3) is not coincidental: the two values differ only in the cell total energies and the elemental reference chemical potentials (Equation (1)), and the μ_{Zn} shifts cancel exactly. The ranking is therefore immune to the precise treatment of the oxygen reference and to any constant

oxygen correction, a property of the formalism that has been emphasised in the defect-calculation literature (Baldassarri et al., 2023). It is, however, a thermodynamic statement about the revPBE energetics of isolated neutral substitutions at 25% concentration; it is not a statement that Mg will spontaneously incorporate under growth conditions. Incorporation also depends on kinetics, including migration barriers, surface desorption and growth rates, none of which are addressed here; and it does not speak to the electrical consequences of doping, which for B1 ZnO have been discussed separately (Goyal & Stevanović, 2018).

Table 3. Formation energies (eV) of pristine, Fe-doped and Mg-doped B1 ZnO.

System	Zn-rich	O-rich
Pristine ZnO (compound, per f.u.)	−4.72	−4.72
Fe_{Zn} (per defect)	+2.20	−2.52
Mg_{Zn} (per defect)	−2.83	−7.55
Δ(Mg − Fe)	−5.03	−5.03

3.7 Zn-rich versus O-rich behaviour

The structure of the limit dependence is simple and exact: as shown in Equation (5), Figures 5 and 6 ($E_f(\text{O-rich}) = E_f(\text{Zn-rich}) + \Delta H_f(ZnO)$) (Momot et al., 2017). With a physical value of ΔH_f=-4.72 eV per formula unit, O-rich conditions lower both defect formation energies by 4.72 eV relative to Zn-rich conditions, reflecting the intuitive fact that under oxygen excess, the ZnO host tolerates cation substitution more readily (the Zn vacancy cost is smaller because Zn atoms are scarce). The relative limit behaviour is identical for Fe-doped and Mg-doped ZnO, so the Fe–Mg formation-energy offset remains consistent and robust. The O-rich absolute values are directly readable, subject to the residual uncertainty of the semi-local oxygen reference discussed in Sections 3.8 and 3.9.

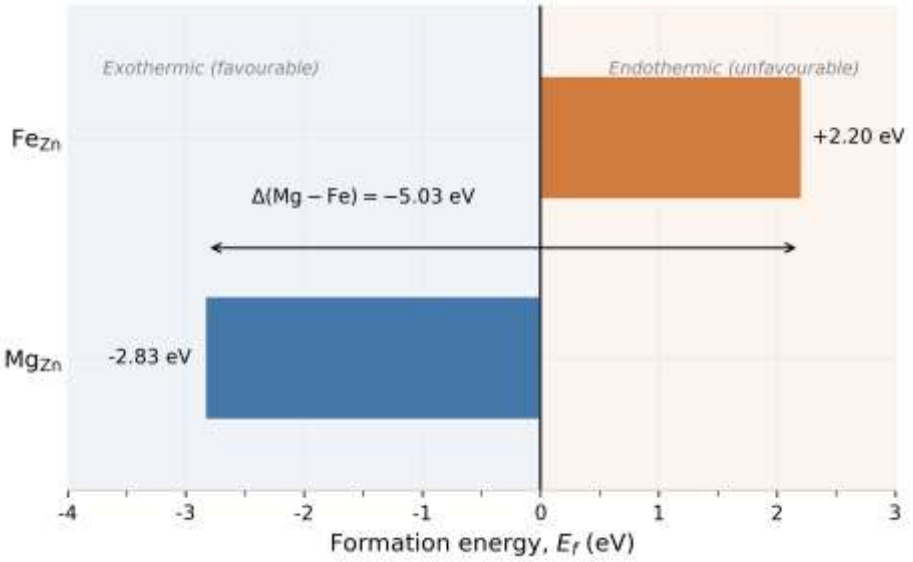

Figure 5. Formation energies of Fe_{Zn} and Mg_{Zn} substitutional defects in rock-salt ZnO at the Zn-rich limit.

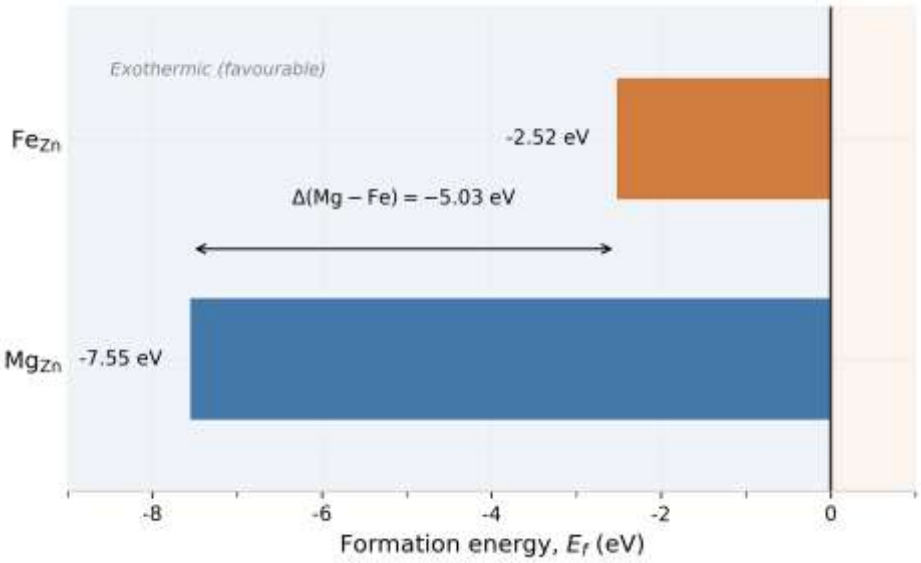

Figure 6. Formation energies of Fe_{Zn} and Mg_{Zn} substitutional defects in rock-salt ZnO at the O-rich limit.

3.8 Effect of oxygen-reference correction

For completeness, we examine the oxygen correction in which the O_2 molecule energy is shifted upward (using Equation (6)) by +1.36 eV per molecule (Youssef & Yildiz, 2012) (the Wang–Maxisch–Ceder fitted procedure (Wang et al., 2006), where a correction of 1.36 eV per O_2 is applied to PBE formation energies (Friedrich et al., 2019)). Because the reference is per atom, the shift is halved:

$$\mu_0^{\text{ref,corr}} = \mu_0^{ref} + \Delta, \Delta = +\frac{1}{2}(1.36eV) = +0.68\text{eV/atom}, \quad (6)$$

That is, numerically $\mu_0^{\text{ref,corr}}$=-436.90506+0.68=-436.22506 eV/atom.

The O-rich chemical potentials must satisfy Equation (3). Since μ_{ZnO} is an SCF output containing no O_2 term, the rise in μ_O forces μ_{Zn} down by the same amount: Equation (7) thus implies that the formation energy at the O-rich limit remains invariant under this oxygen correction, as the shifting potentials of the oxygen and zinc species perfectly compensate for the underlying shift in the O_2 reference.

$$\mu_{Zn}^{\text{O-rich,corr}} = \mu_{ZnO} - \mu_0^{\text{ref,corr}} = \mu_{Zn}^{\text{O-rich}} - 0.68\text{eV/atom} = -6183.12723\text{eV/atom}. \quad (7)$$

Because only μ_{Zn} changes under the correction, and only at the O-rich limit, substituting the corrected μ_{Zn} into Equation (1) gives Equation (8).

$$E_f^{corr}(X_{Zn})^{\text{O-rich}} = E_f(X_{Zn})^{\text{O-rich}} - 0.68eV. \quad (8)$$

At the Zn-rich limit, $\mu_{Zn} = \mu_{Zn}^{ref}$ is the SCF energy of the Zn cell alone, which contains no O_2-referenced quantity; hence $E_f(\text{Fe}_{\text{Zn}}) = +2.20$ eV and $E_f(\text{Mg}_{\text{Zn}}) = -2.83$ eV are invariant under the correction. The compound formation enthalpy shifts by the same amount (Equation (9)) (Friedrich et al., 2019):

$$\Delta H_f^{corr} = \Delta H_f - 0.68 = -4.72 - 0.68 = -5.40\text{eV/f.u.} \quad (9)$$

Note the sign: the corrected ΔH_f is *more* negative (−5.40 eV), i.e., further from the experimental wurtzite formation enthalpy of about −3.6 eV (Itoh & Azakami, 1989), not closer to it. In the present dataset, the standard fitted O_2 correction therefore does not improve the agreement with experiment, and the uncorrected SCF values remain the primary results. This behaviour is a direct consequence of the already strongly negative, per-atom-normalised reference chain and illustrates why fitted corrections, being tuned to specific functionals, pseudopotentials and fitting sets, are not transferable without refitting (Stevanović et al., 2012); in particular, the +1.36 eV shift was fitted to PBE total energies (Friedrich et al., 2019), whereas the present pseudopotentials are based on the revPBE functional (Hammer et al., 1999). What the correction does preserve by its constant-shift property (Baldassarri et al., 2023) is every energy difference: the Mg–Fe offset from Equation (5) and all Zn-rich values, which are exactly unchanged.

Table 4. Oxygen-reference correction at the O-rich limit (consistent normalisation).

Quantity	Uncorrected revPBE/ eV	Corrected(+0.68 eV on μ_O)/ eV	Δ(corrected)/ eV
μ_O^{ref} (eV/atom)	-436.91	-436.23	0.68
$\mu_{Zn}^{O\text{-}rich}$ (eV/atom)	-6182.45	-6183.13	-0.68
ΔH_f (eV/f.u.)	-4.72	-5.4	-0.68
$E_f(Fe_{Zn})$, O-rich (eV)	-2.52	-3.2	-0.68
$E_f(Mg_{Zn})$, O-rich (eV)	-7.55	-8.23	-0.68

The O-rich results above rest on the per-atom normalisation of the oxygen reference (cell energy ÷ 8). Because the algebraic chain of Equations (1), (2), (3) and (4), which is satisfied for any internally consistent choice of μ_0, cannot by itself detect an error in the reference normalisation, the reference chain must additionally reproduce the physical scale of ΔH_f (≈ −3 to −4 eV/f.u. for ZnO) and of $\frac{1}{2}E(O_2)$. To document this, Table 5 reproduces what happens if the oxygen cell energy is divided by 16 instead of 8 (an extra factor ½ on the per-atom reference, μ_0=-218.45253 eV/atom: ΔH_f plummets to −223.17 eV/f.u., and the O-rich defect formation energies become −220.98 eV (Fe_{Zn}) and −226.01 eV (Mg_{Zn}); values on this scale are 60 times more negative than the experimental −3.6 eV/f.u. (Erhart et al., 2006). They are diagnostic of a reference-normalisation artefact, not of physical instability, and no constant correction can repair them (the +0.68 eV shift leaves them at −221.66 and −226.69 eV, respectively). The internal consistency of the dataset is therefore verified by two independent checks: (i) the reference values satisfy Equation (4) exactly, and (ii) the O-rich defect energies in Tables 3 and 4 lie on the physical defect-energy scale.

Table 5. Diagnostic: effect of a spurious factor ½ in the oxygen-reference normalisation.

Quantity	Consistent normalisation (÷8)/ eV	Inconsistent normalisation (÷16)/ eV	After +0.68 eV correction (consistent / inconsistent normalisation)/ eV
μ_O^{ref} (eV/atom)	-436.91	-218.45	−436.22506 / −217.77253
μ_Zn^O-rich (eV/atom)	-6182.45	-6400.9	−6183.12723 / −6401.57976
ΔH_f (eV/f.u.)	-4.72	-223.17	−5.40 / −223.85
E_f(Fe_Zn), O-rich (eV)	-2.52	-220.98	−3.20 / −221.66
E_f(Mg_Zn), O-rich (eV)	-7.55	-226.01	−8.23 / −226.69

Two conclusions follow. First, the per-atom-normalised SCF reference places ΔH_f on the physical oxide scale (−4.72 eV/f.u.), and every quantity derived from it the stability window, the O-rich defect energies, and the Mg–Fe ordering—is internally consistent; the standard +1.36 eV per-O_2 correction shifts ΔH_f by −0.68 eV/f.u. (to −5.40 eV) and the O-rich defect energies by −0.68 eV each, without affecting any difference or ranking (Baldassarri et al., 2023). Second, corrections of this type are fitted quantities

(Stevanović et al., 2012), not transferable to the present revPBE setup without re-fitting (Youssef & Yildiz, 2012). We therefore report the raw SCF results in full and evaluate the standard correction here only to document its effect on the present data and to demonstrate that the reference chain passes the scale checks of Table 5. Subsequent analysis of Fe and Mg doping focuses on these raw energies, as they provide the most reliable thermodynamic baseline for examining vacancy formation and lattice stability (Hoang & Johannes, 2014).

3.9 Limitations and physical interpretation

All calculations are spin-unresolved (Section 2.3). Octahedrally coordinated Fe^{2+} is an open-shell 3d ion whose expected ground state is high-spin (S = 2) (Marcondes et al., 2020); the non-magnetic solution removes the majority–minority exchange splitting. The sign of the resulting bias is not a priori predictable, because magnetic stabilisation of the doped cell would lower E_f (Fe_{Zn}) whereas that of the magnetically ordered Fe metal reference would raise it. Spin-polarised GGA+U or hybrid verification of the Fe values is therefore recommended (Freysoldt et al., 2014; Wang et al., 2006), since semi-local functionals misplace transition-metal d states (Dietl & Ohno, 2014). Mg^{2+}, being closed-shell and magnetically inert, requires no such qualification (Tampul et al., 2026).

The remaining domain of validity is unchanged: neutral 25% substitution in an eight-atom periodic B1 cell at 0 K, revPBE with its inherited semi-local band-gap underestimation, and an O_2-overbinding uncertainty of approximately 0.5 eV–1 eV per oxygen atom in absolute O-rich values. The per-atom ÷8 oxygen normalisation passes the scale checks of Section 3.8, an erroneous ÷16 yields ΔH_f approximately −223 eV/f.u. and O-rich defect energies approximately −221 to −227 eV, about 60× the experimental −3.6 eV/f.u. (Itoh & Azakami, 1989) and dopant–dopant, finite-size, charged-state, entropic and kinetic effects remain outside this scope.

4. Conclusion

The study answered quantitatively which dopant, Fe or Mg, is thermodynamically more accessible on the Zn site of rock-salt (B1) ZnO: the pristine host formation energy emerged as eV per formula unit, close to the experimental wurtzite value of about eV per formula unit (Erhart et al., 2006); Fe substitution is endothermic at the Zn-rich limit, eV, whereas Mg substitution is exothermic, eV, and at the O-rich limit the corresponding values are eV and eV. The approximately 5 eV gap between the dopants has a clear chemical origin. The stronger Mg–O bonding, reflected in the greater stability of MgO than ZnO relative to their respective elemental references, is the same driving force that places the wurtzite-to-rock-salt boundary at in $Mg_xZn_{1-x}O$ (Ohtomo et al., 1999), whereas Fe substitution on the octahedrally coordinated Zn site of the B1 host is comparatively thermodynamically less accessible within the framework. At 0 K, equilibrium thermodynamics therefore predicts Mg incorporation in B1 ZnO to be far more favourable than Fe incorporation, a conclusion that rests on differences in which systematic reference errors cancel exactly; the standard eV per O_2 molecule correction (Friedrich et al., 2019) shifts to eV/f.u. and the O-rich defect energies by eV each but does not affect any ordering.

Data Availability Statement

The DFT parameters and SCF total energies underlying this study are reported in the tables of this article (Tables 1, 2, and 5). The calculations were performed with the open-source Quantum ESPRESSO package under the thermo_pw workflow; input files (including pseudopotential identifiers, which are required for exact reproduction) are available from the authors on reasonable request.

Declaration of Competing Interests

The authors declare that they have no known competing financial interests or personal relationships that could be perceived to influence the work reported in this paper.

REFERENCES

Abdel-Baset, T. A., Fang, Y., Anis, B., Duan, C., & Abdel-Hafiez, M. (2016). *Structural and Magnetic Properties of Transition-Metal-Doped Zn 1−x Fe x O*. https://doi.org/10.1186/s11671-016-1332-x

Ahmedbowba, S., Khadri, F., Ouerghui, W., & Ridene, S. (2025). New investigation of the electronic and structural properties of (Mg,Ti)-doped and co-doped ZnO structures: A DFT and DFT+U study. *ArXiv.Org*. http://arxiv.org/abs/2503.02731

Baldassarri, B., He, J., Qian, X., Mastronardo, E., Griesemer, S., Haile, S. M., & Wolverton, C. (2023). Accuracy of DFT computed oxygen-vacancy formation energies and high-throughput search of solar thermochemical water-splitting compounds. *American Physical Society: Phys. Rev. Materials*, *7*(6), 65403. https://doi.org/10.1103/physrevmaterials.7.065403

Bartók, A. P., & Yates, J. R. (2019). *Ultrasoft pseudopotentials with kinetic energy density support: Implementing the Tran-Blaha potential*. https://doi.org/10.1103/physrevb.99.235103

Corso, A. D. (2014). *Pseudopotentials periodic table: From H to Pu*. https://doi.org/10.1016/j.commatsci.2014.07.043

Dietl, T., & Ohno, H. (2014). *Dilute ferromagnetic semiconductors: Physics and spintronic structures*. https://doi.org/10.1103/revmodphys.86.187

Doerksen, E. S., & Fortenberry, R. C. (2020). Coincidence between Bond Strength, Atomic Abundance, and the Composition of Rocky Materials. *ACS Earth and Space Chemistry*, *4*(6), 812–817. https://doi.org/10.1021/acsearthspacechem.0c00029

Drissi, N., Gueddim, A., & Bouarissa, N. (2020). *First-principles study of rocksalt MgxZn1− xO: band structure and optical spectra*. https://doi.org/10.1080/14786435.2020.1727974

Erhart, P., Albe, K., & Klein, A. (2006). First-principles study of intrinsic point defects in ZnO: Role of band structure, volume relaxation, and finite-size effects. *Physical Review B*, *73*(20). https://doi.org/10.1103/physrevb.73.205203

Freysoldt, C., Grabowski, B., Hickel, T., Neugebauer, J., Kresse, G., Janotti, A., & Walle, C. G. V. de. (2014). *First-principles calculations for point defects in solids*. https://doi.org/10.1103/revmodphys.86.253

Friedrich, R., Usanmaz, D., Oses, C., Supka, A., Fornari, M., Nardelli, M. B., Toher, C., & Curtarolo, S. (2019). Coordination corrected ab initio formation enthalpies. *Nature Partner Journals Computational Materials in Partnership with the Shanghai Institute of Ceramics of the Chinese Academy of Sciences*. https://doi.org/10.1038/s41524-019-0192-1

Ganguli, N., Dasgupta, I., & Sanyal, B. (2009). *The making of ferromagnetic Fe doped ZnO nanoclusters*. https://doi.org/10.1063/1.3136904

Gerward, L., & Olsen, J. S. (1995). *The High-Pressure Phase of Zincite*. https://doi.org/10.1107/s0909049595009447

Giannozzi, P., Andreussi, O., Brumme, T., Bunau, O., Nardelli, M. B., Calandra, M., Car, R., Cavazzoni, C., Ceresoli, D., Cococcioni, M., Colonna, N., Carnimeo, I., Corso, A. D., Gironcoli, S. de, Delugas, P., DiStasio, R. A., Ferretti, A., Floris, A., Fratesi, G., … Baroni, S. (2017). *Advanced capabilities for materials modelling with Quantum ESPRESSO*. https://doi.org/10.1088/1361-648x/aa8f79

Giannozzi, P., Baroni, S., Bonini, N., Calandra, M., Car, R., Cavazzoni, C., Ceresoli, D., Chiarotti, G., Cococcioni, M., Dabo, I., Corso, A. D., Gironcoli, S. de, Fabris, S., Fratesi, G., Gebauer, R., Gerstmann, U., Gougoussis, C., Kokalj, A., Lazzeri, M., … Wentzcovitch, R. M. (2009). *QUANTUM ESPRESSO: a modular and open-source software project for quantum simulations of materials*. https://doi.org/10.1088/0953-8984/21/39/395502

Goyal, A., & Stevanović, V. (2018). *Metastable rocksalt ZnO is p-type dopable*. https://doi.org/10.1103/physrevmaterials.2.084603

Hammer, B., Hansen, L. B., & Nørskov, J. K. (1999). Improved adsorption energetics within density-functional theory using revised Perdew-Burke-Ernzerhof functionals. *American Physical Society*, *59*(11), 7413–7421. https://doi.org/10.1103/physrevb.59.7413

Hoang, K., & Johannes, M. D. (2014). Defect chemistry in layered transition-metal oxides from screened hybrid density functional calculations. *arXiv (Cornell University)*, *2*(15), 5224–5235. https://doi.org/10.1039/c4ta00673a

Hohenberg, P. C., & Kohn, W. (1964). *Inhomogeneous Electron Gas*. https://doi.org/10.1103/physrev.136.b864

Itoh, S., & Azakami, T. (1989). *Thermodynamic Studies of ZnO in Solid Zinc Silicate*. https://doi.org/10.2473/shigentosozai.105.685

Kohn, W., & Sham, L. J. (1965). *Self-Consistent Equations Including Exchange and Correlation Effects*. https://doi.org/10.1103/physrev.140.a1133

Marcondes, M. L., Zheng, F., & Wentzcovitch, R. M. (2020). Phonon dispersion throughout the iron spin crossover in ferropericlase. *arXiv (Cornell University)*, *102*(10). https://doi.org/10.1103/physrevb.102.104112

Maznichenko, I. V., Ernst, A., Bouhassoune, M., Henk, J., Däne, M., Lüders, M., Bruno, P., Hergert, W., Mertig, I., Szotek, Z., & Temmerman, W. M. (2009). *Structural phase transitions and fundamental band gaps ofMgxZn1−xOalloys from first principles*. https://doi.org/10.1103/physrevb.80.144101

Mellan, T. A., & Grau-Crespo, R. (2012). *Density functional theory study of rutile VO2 surfaces*. https://doi.org/10.1063/1.4758319

Meyer, B. (2004). *First-principles study of the polar O-terminated ZnO surface in thermodynamic equilibrium with oxygen and hydrogen*. https://doi.org/10.1103/physrevb.69.045416

Momot, A., Amini, M. N., Reekmans, G., Lamoen, D., Partoens, B., Slocombe, D. R., Elen, K., Adriaensens, P., Hardy, A., & Bael, M. K. V. (2017). *A novel explanation for the increased conductivity in annealed Al-doped ZnO: an insight into migration of aluminum and displacement of zinc*. https://doi.org/10.1039/c7cp02936e

Muller, A., Comas-Vives, A., & Coperet, C. (2022). Ga and Zn increase the oxygen affinity of Cu-based catalysts for the COx hydrogenation according to ab initio atomistic thermodynamics. *Royal Society of Chemistry Chemical Science*, 13442–13458. https://doi.org/10.1039/d2sc03107h

Ohtomo, A., Shiroki, R., Ohkubo, I., Koinuma, H., & Kawasaki, M. (1999). *Thermal stability of supersaturated MgxZn1−xO alloy films and MgxZn1−xO/ZnO heterointerfaces*. https://doi.org/10.1063/1.125545

Özgür, Ü., Alivov, Ya. I., Liu, C., Teke, A., Reshchikov, M. A., Doğan, S., Avrutin, V., Cho, S.-J., & Morkoç, H. (2005). *A comprehensive review of ZnO materials and devices*. https://doi.org/10.1063/1.1992666

Perdew, J. P., Burke, K., & Ernzerhof, M. (1996). *Generalized Gradient Approximation Made Simple*. https://doi.org/10.1103/physrevlett.77.3865

Petretto, G., & Bruneval, F. (2014). *ComprehensiveAb InitioStudy of Doping in Bulk ZnO with Group-V Elements*. https://doi.org/10.1103/physrevapplied.1.024005

Raha, S., & Ahmaruzzaman, Md. (2022). *ZnO nanostructured materials and their potential applications: progress, challenges and perspectives*. https://doi.org/10.1039/d1na00880c

Recio, J. M., Blanco, M. A., Luaña, V., Pandey, R., Gerward, L., & Olsen, J. S. (1998). *Compressibility of the high-pressure rocksalt phase of ZnO*. https://doi.org/10.1103/physrevb.58.8949

Sakong, S., Gutjahr, J., & Kratzer, P. (2013). Comparison of density functionals for nitrogen impurities in ZnO. *arXiv (Cornell University)*, *138*(23), 234702. https://doi.org/10.1063/1.4810862

Santana, J. A., Krogel, J. T., Kim, J., Kent, P. R. C., & Reboredo, F. A. (2015). *Structural stability and defect energetics of ZnO from diffusion quantum Monte Carlo*. https://doi.org/10.1063/1.4919242

Schmidt-Mende, L., & MacManus-Driscoll, J. L. (2007). *ZnO – nanostructures, defects, and devices*. https://doi.org/10.1016/s1369-7021(07)70078-0

Segura, A., Sans, J. A., Manjón, F. J., Muñoz, A., & Herrera-Cabrera, M. J. (2003). *Optical properties and electronic structure of rock-salt ZnO under pressure*. https://doi.org/10.1063/1.1591995

Sharikov, F. Yu., Соколов, П. С., Баранов, А. Н., & Solozhenko, V. L. (2017). *On the thermodynamic aspect of zinc oxide polymorphism: calorimetric study of metastable rock salt ZnO*. https://doi.org/10.1016/j.mencom.2017.11.025

Stevanović, V., Lany, S., Zhang, X., & Zunger, A. (2012). Correcting density functional theory for accurate predictions of compound enthalpies of formation: Fitted elemental-phase reference energies. *American Physical Society*, *85*(11), 115104–115116. https://doi.org/10.1103/physrevb.85.115104

Tampul, H., Sani, F., & Moreh, A. U. (2026). *A Review on the Effects of Fe and Mg Doping on the Properties of ZnO Nanomaterials: A DFT Perspective*. https://doi.org/10.33003/fjs-2026-1014-5734

Utrera-Barrios, S., Steenackers, N., Terryn, S., Ferrentino, P., Verdejo, R., Assche, G. V., López-Manchado, M. A., Brancart, J., & Santana, M. H. (2023). *Unlocking the potential of self-healing and recyclable ionic elastomers for soft robotics applications*. https://doi.org/10.1039/d3mh01312j

Walle, C. G. V. de, & Neugebauer, J. (2004). *First-principles calculations for defects and impurities: Applications to III-nitrides*. https://doi.org/10.1063/1.1682673

Wang, L., Maxisch, T., & Ceder, G. (2006). *Oxidation energies of transition metal oxides within theGGA+Uframework*. https://doi.org/10.1103/physrevb.73.195107

Yim, K., Lee, J., Lee, D.-H., Lee, M., Cho, E., Lee, H. S., Nahm, H., & Han, S. (2017). *Property database for single-element doping in ZnO obtained by automated first-principles calculations*. https://doi.org/10.1038/srep40907

Youssef, M., & Yildiz, B. (2012). *Intrinsic point-defect equilibria in tetragonal ZrO2: Density functional theory analysis with finite-temperature effects*. https://doi.org/10.1103/physrevb.86.144109

Zhang, S., & Northrup, J. E. (1991). *Chemical potential dependence of defect formation energies in GaAs: Application to Ga self-diffusion*. https://doi.org/10.1103/physrevlett.67.2339